Research Article

# Synthesis of metal–organic frameworks (MOFs) MIL-100(Fe) functionalized with thioglycolic acid and ethylenediamine for removal of eosin B dye from aqueous solution

Adedibu C. Tella[1,2] · Janet T. Bamgbose[2] · Vincent O. Adimula[1] · Mary Omotoso[1] · Sunday E. Elaigwu[1] · Victoria T. Olayemi[1,3] · Olusegun A. Odunola[2]

## Abstract

The interaction of eosin B dye from aqueous solution with MIL-100(Fe) and functionalized MIL-100(Fe) metal–organic frameworks (MOFs) is reported in this study. MIL-100(Fe) was prepared and functionalized with thioglycolic acid (TH) and ethylenediammine (ED) separately by incorporating the thiol (–SH) and the amine (–NH$_2$) group of the functionalizing agents into the open metal sites of the MIL-100(Fe) to obtain the acidic (TH-MIL-100) and basic (ED-MIL-100) forms of the MOF respectively. Characterization of the MOFs was done by melting point analysis, elemental analysis, spectroscopic techniques, scanning electron microscopy (SEM), and powdered X-ray diffraction (PXRD) analysis. The adsorption experiments were carried out at different conditions such as pH, adsorbent dosage, contact time, temperature, and initial concentration of the dye to estimate the optimum conditions and the maximum adsorption capacities. Adsorption capacities were observed to increase in the order of ED-MIL-100 < MIL-100 < TH-MIL-100, while the TH-MIL-100 was the most effective in the removal process due to acid–base interaction between the acidic thiol group (–SH) and the alkaline medium of eosin B dye solution. The Langmuir Isotherm was seen to fit well to adsorption data obtained for all three adsorbent materials studied, and adsorption processes followed the pseudo-second order kinetics. This study, therefore, indicates the suitability of functionalization of MIL-100(Fe) towards improving its adsorption capacity.

**Keywords** MIL-100(Fe) · Functionalization · Eosin B · Characterization · Adsorption

## 1 Introduction

Porous coordination polymers (Metal–organic frameworks (MOFs)) have been presented as emerging materials showing high degree of porosity and extensively studied due to unique characteristics which include structural flexibility and rigidity, high degree of pore volume, and their uniquely high specific surface area [1]. The internal surfaces of MOFs are also susceptible to tuning to achieve the desired characteristics enabling their preparation for specific purposes [1, 2]. MOFs having rigid structures which possess pores that are well-defined having internal diameters of up to about 48 Å are able to present large free spaces which could accommodate guest molecules achieving MOFs that are applicable for the purpose of energy storage [3, 4], adsorption and separation processes [5], in-pore assembly of nano particles [6, 7], catalytic processes [8, 9], and drug loading/delivery [10–13].

The functionalization of MOFs which is otherwise referred to as post synthetic modification enables the altering of MOFs surfaces by the introduction of functional groups on to the MOFs which changes the pore

✉ Vincent O. Adimula, vincentadimula@gmail.com | [1]Laboratory of Synthetic Inorganic and Materials Chemistry, Department of Chemistry, University of Ilorin, Ilorin, Nigeria. [2]Department of Chemistry, Hallmark University, Ogun state, Ijebu-Itele, Nigeria. [3]Department of Chemistry, College of Pure and Applied Sciences, Kwara State University, P.M.B. 1530, Malete, Nigeria.

functionality of MOF, which results in selective interactions of the pores with guest molecules. The large number of available ligands with a variety of functionalities have enabled the achievement of MOFs having a variety of functional groups. However, synthesis processes using these ligands alone sometimes do not achieve the desired functionalities or MOF structure in these materials, hence, it becomes imperative in this case to develop alternative routes such as functionalization to achieve desired MOF properties by interacting the functional groups on the ligands with post synthetic functionalizing agents to generate MOFs having the desired characteristics [14, 15]. The MIL-100(Fe) MOF is a crystalline three-dimensional material prepared from a combination of iron(III) salt and the tricarboxylate ligand (trimesic acid) and this material has been reported as one of the highly porous MOFs available. The two mesoporous cage sets (24 and 29 Å) are reportedly accessible through the microporous windows (ca.8.6 Å and ca.4.7–5.5 Å) of the material [16, 17], and the non-toxic nature of the $Fe^{3+}$ ion which is inexpensive and environmentally friendly gives the MIL-100(Fe) its importance and desirability.
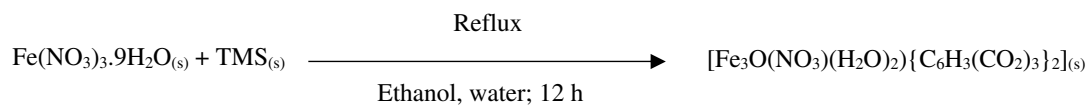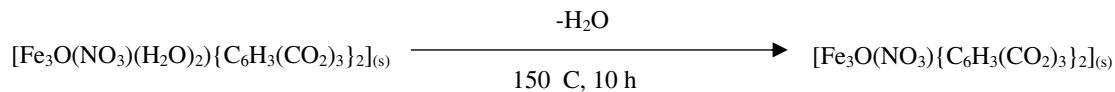
Synthetic dyes such as methyl red, malachite green, and eosin B, have been utilized as essential starting materials for colouring purposes in various industrial processes ranging from printing, textiles, cosmetics, and leather. However, the widespread use of this organic dyes has led to their increased discharge into environmental medias which poses significant danger to life and the environment due to their toxic nature at elevated concentrations. Technologies and procedures have been designed with the aim of removing these toxic substances from the environment. Utilized procedures for removing dyes from the environment include biological treatment, membrane filtration method, and adsorption. The adsorption procedure is reported to be the most widespread used technique for environmental remediation of dyes due to its effectiveness and good colour removal potential. Materials such as zeolites and activated carbon have been used as adsorbents for the removal process, however, their use for dye removal have been restricted due to small pore diameter which limits efficiency of dye adsorption [18, 19]. Hamedi et al. [18, 19] prepared new MOF composite of MIL-101(Fe)@PDopa@$Fe_3O_4$ and MIL-100(Fe)@$Fe_3O_4$@AC nanocomposite for the removal of methyl red (MR), malachite green (MG), and rhodamine B (RhB) dye pollutants from the environment. The MIL-101(Fe)@PDopa@$Fe_3O_4$ adsorption capacity was obtained to be 1250 mg/g at 298 K for MR and 833 mg/g at 318 K for MG and observed to be of better efficiency than other adsorbents. The ability of the prepared MIL-100(Fe)@$Fe_3O_4$@AC to adsorb RhB dye was observed to be 769.23 mg/g, and also found to be higher than other adsorbents which has been utilized for the same process.
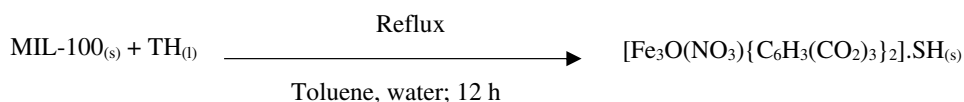
Interestingly, an effective assembly strategy via the pre-modification of organic ligands and/or post-modification of prepared MOFs is important for the construction of novel MOFs which have found application in several processes [20] including dye encapsulation [21]. Hong et al. [22] prepared a series of mesoporous Zn-MOFs by coordinating zinc(II) ion with of 9-fluorenone-2,7-dicarboxylic acid ($H_2$FDCA), dibenzo[b,d]thiophene-3,7-dicarboxylic acid 5,5-dioxide ($H_2$DTDAO), and fluorene-2,7-dicarboxylic acid ($H_2$FDC) which were utilized as adsorbents for the removal of methylene blue (MB) from aqueous media, and reported that the Zn-MOFs were observed to be excellent adsorbents for the removal of MB. Masoomi et al. [23] investigated the photocatalytic activity of three Zn(II) MOFs formulated as TMU-4, TMU-5, and TMU-6 which were prepared by a mechanochemical technique, in the decolorization of the congo red dye. It was observed that the photocatalysts were also able to mineralize and degrade the dye even in the absence of oxidants such as $H_2O_2$. Abdollahi et al. [24] also prepared a new Zn-MOF, and formulated as TNU-39, by the ultrasonic irradiation and solvothermal techniques, and investigated the ability of this MOF in the removal of congo red (CR) and sudan red (SR) dyes. It was observed that removal efficiency for SR was higher than that of CR and attributed this to the smaller size of the SR dye molecules.

The eosin B dye is reported to be a very reactive organic dye with hazardous effects in the environment [25]. The combination of this dye with other synthetic dyes for domestic and industrial purposes has seen a considerable increase over the last decades. These dyes are employed in the manufacture of materials such as clothing, paper, leather, amongst others to achieve colourful designs and to make these items attractive. Wastes generated from the use of these dyes are usually discarded indiscriminately thereby polluting the environment in the process [1–4]. These effluents usually are able to block sunlight and oxygen from penetrating into water bodies depriving aquatic forms of life the essential ingredients of their survival. Also, these dyes can undergo degradation into compounds which have the potential of being carcinogenic and end up in the food chain [26, 27] necessitating the need to urgently remove these chemicals from wastewater before discharge [16].
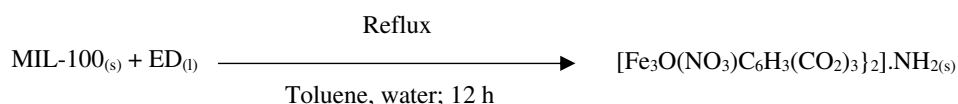
This work focuses on functionalization of MIL-100(Fe) by incorporating the thio- and amine- functional groups unto the prepared MIL-100(Fe) using thioglycolic acid and ethylenediamine thereby achieving new functionalized MIL-100(Fe) materials as a platform for environmental remediation of dyes. The ability of these functionalized MIL-100(Fe) materials to adsorb and remove the eosin B

$$Fe(NO_3)_3.9H_2O_{(s)} + TMS_{(s)} \xrightarrow[\text{Ethanol, water; 12 h}]{\text{Reflux}} [Fe_3O(NO_3)(H_2O)_2]\{C_6H_3(CO_2)_3\}_2]_{(s)}$$

**Scheme 1** Equation of reaction for synthesis of MIL-100(Fe)

$$[Fe_3O(NO_3)(H_2O)_2]\{C_6H_3(CO_2)_3\}_2]_{(s)} \xrightarrow[\text{150 C, 10 h}]{-H_2O} [Fe_3O(NO_3)\{C_6H_3(CO_2)_3\}_2]_{(s)}$$

**Scheme 2** Equation of reaction for dehydration of MIL-100(Fe)

**Scheme 3** Equation of reaction for functionalization of MIL-100 using thioglycolic acid

$$MIL\text{-}100_{(s)} + TH_{(l)} \xrightarrow[\text{Toluene, water; 12 h}]{\text{Reflux}} [Fe_3O(NO_3)\{C_6H_3(CO_2)_3\}_2].SH_{(s)}$$

**Scheme 4** Equation of reaction for functionalization of MIL-100 using ethylenediamine

$$MIL\text{-}100_{(s)} + ED_{(l)} \xrightarrow[\text{Toluene, water; 12 h}]{\text{Reflux}} [Fe_3O(NO_3)C_6H_3(CO_2)_3\}_2].NH_{2(s)}$$

dye from the environment is studied. To the best of our knowledge, there is limited information on functionalization of MIL-100(Fe) and particularly with thioglycolic acid and ethylenediamine for use in the removal of eosin B dye. Thus, we report the preparation and functionalization with thioglycolic acid and ethylendiamine of MIL-100(Fe) and their use as adsorbents for the removal of eosin B dye from aqueous media.

## 2 Experimental procedure

Iron(III) nitrate nonahydrate (99%), trimesic acid (99%), thioglycolic acid (98%), ethanol (98%), and ethylenediamine (98%) were obtained from Sigma Aldrich Co., Germany, and used without further purification.

### 2.1 Synthesis of MIL-100(Fe) adsorbents

The MIL-100 was synthesized based on method previously described [17, 28]. Iron(III) nitrate nonahydrate (10 mmol, 4.04 g) was weighed and dissolved in 50 ml of deionized water, 9 mmol (1.89 g) of trimesic acid was also weighed and dissolved separately in 50 ml of ethanol. The solutions were mixed together and refluxed for 12 h at 95 °C. Precipitate formed was filtered, washed with deionized water/ ethanol (50:50), and dried at room temperature. Thereafter,

it was activated in a vacuum oven at 150 °C for 10 h, and stored in a desiccator.

Functionalization of the synthesized MIL-100 was carried out by modifications to a previously reported procedure [29]. For the TH-MIL-100, 0.3 g of the dehydrate MIL-100(Fe) was weighed into 10 ml of anhydrous toluene and 1 ml of thioglycolic acid (TH) was added to the suspension. This mixture was continuously refluxed at 120 °C for 12 h to obtain an optimized grafting, and the resulting solid was washed severally with deionized water/ethanol (50:50), dried at room temperature, and stored in a desiccator. The same procedure described above was followed for the preparation of the ED-MIL-100, however, thioglycolic acid was replaced with ethylenediamine (ED). The equation of reactions is presented in Schemes 1, 2, 3, 4 below.

### 2.2 Characterization of the MOFs

The melting points of the MOFs were determined using a Gallen-Kamp melting point apparatus. Elemental analysis was performed on a Perkin-Elmer CHN Analyzer 2400 series II. UV–Visible measurements were performed on a SHIMADZU UV-1650 UV–VIS spectrophotometer. Fourier transform infrared (FT-IR) analysis was performed using a SHIMADZU scientific model FTIR 8400 s spectrophotometer. Brunauer–Emmett–Teller surface area analysis was carried out using NOVA 4200e BET instrument.

## 2.3 Adsorption studies

Adsorption studies were carried out following a procedure previously reported by [30–33]. Adsorption of eosin B dye onto the adsorbents (MIL-100(Fe), TH-MIL-100, and ED-MIL-100) was studied using eosin B stock solution of 1000 mg/L. This was prepared by dissolving 0.1 g of the eosin B dye in 1000 ml of deionized water. Lower concentrations of the dye (5–30 mg/L) were prepared from the stock solution by serial dilution with deionized water, and the concentration of eosin B determined from absorbance measurement at $\lambda_{max}$ of 530 nm using a SHIMADZU UV-1650pc Ultraviolet–Visible (UV–Vis) spectrophotometer. The calibration curve (Fig. 1) was plotted using absorbance values obtained from the eosin B working standards of 5–30 mg/L.

Before adsorption study, the MIL-100 was dried for 12 h at 150 °C. The activated MIL-100(Fe) and functionalized MIL-100 adsorbents (0.02 g of each) were then added to the prepared solutions separately and the mixtures were shaken for 2 h. Absorbance readings were taken using the UV–Visible spectrophotometer (SHIMADZU UV-1650pc Ultraviolet–Visible (UV–Vis) spectrophotometer) at a $\lambda_{max}$ of 530 nm. The effect of concentration, temperature, time, pH, and adsorbent dosage on the adsorption process was also determined and absorbance before and after the adsorption process was taken to determine the quantity ($q_e$) of eosin B (mg/g) dye adsorbed at equilibrium using the formula:

$$q_e = \left( \frac{C_o - C_e}{m} \right) v \tag{1}$$

where $C_o$ and $C_e$ (mg/L) are the initial and final concentrations of the adsorbates respectively, v is the volume of the solution used (ml) and m is the mass (g) of the adsorbents. The effect of time was studied at time interval of 30–180 min, while the effect of temperature was studied at temperature range of 30–70 °C. The effect of pH was studied by varying the pH between 2 and 13 using 0.1 M HCl or 0.1 M NaOH, while the effect of adsorbent dosage was studied using 0.01–0.05 g of the adsorbents, and the effect of concentration was studied using 5–30 mg/L of the adsorbate.
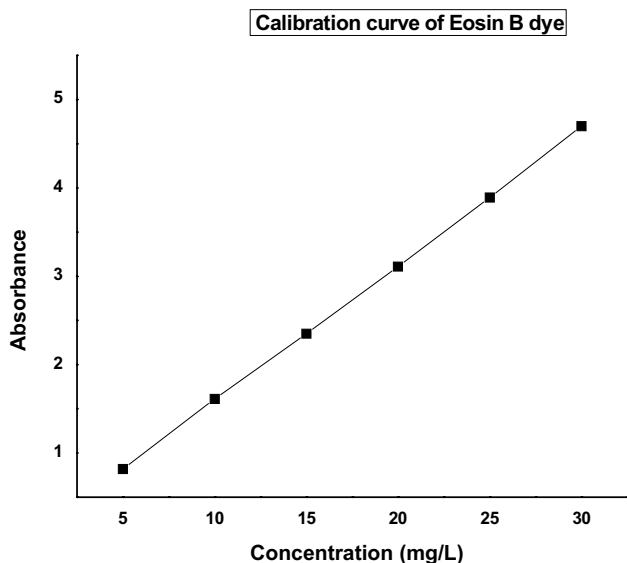
## 3 Result and discussion

### 3.1 Characterization of MIL-100 adsorbents

Physico-chemical parameters and elemental analysis of the MIL-100, TH-MIL-100, and ED-MIL-100 prepared are presented in Table 1. The melting point of MIL-100 prepared was observed to increase after functionalization.

### 3.2 Spectroscopic analysis

The Fourier-transform infrared (FT-IR) spectrum of the synthesized MIL-100 in this study was compared with previously reported spectrum of the MOF [27]. The pattern shows bands at 3430, 1720, 1382 and 1450 cm$^{-1}$ correlated with the 3500, 1720, 1350, and 1480 cm$^{-1}$ of the previous report [27]. A 0.195 g yield was obtained for the TH-MIL-100 representing a 65% yield, and the FT-IR spectrum of the functionalized MIL-100 with thioglycolic was found to be similar to that of the synthesized MIL-100, with



**Fig. 1** Calibration curve showing the plot of absorbance against $C_o$ of eosin B

**Table 1** Physicochemical analysis of the MIL-100, TH-MIL-100, and ED-MIL-100

| Adsorbent | Elemental analysis results % found (calc.) | | | | % Yield | Melting point (°C) |
|---|---|---|---|---|---|---|
| | C | H | N | S | | |
| MIL-100 | 22.5 (20.6) | 2.98 (2.11) | 2.68 (2.67) | – | 75% | 281 |
| TH-MIL-100 | 30.48 (30.37) | 2.55 (2.74) | – | 12.33 (12.01) | 65% | 318 |
| ED-MIL-100 | 15.46 (16.15) | 3.92 (3.01) | 10.36 (10.99) | – | 75% | 363 |

additional bands owing to coordination between the MIL-100 and the functionalizing agent. The presence of these new bands was further confirmed by comparing them with the spectrum of a thiol functionalized MOF reported by [30]. The synthesized TH-MIL-100 showed additional bands at 3000, 2659, and 621 $cm^{-1}$ correlating with the thiol functionalized MOF reported by [30], which are 2900, 2581 and 686 $cm^{-1}$ assigned to $\upsilon(C–H)$, $\upsilon(S–H)$, and $\upsilon(C-S)$ vibrations respectively. The yield obtained for the ED-MIL-100 was calculated to be 0.225 g, representing a 75% yield. The FT-IR spectrum of the functionalized ED-MIL-100 is also similar to the synthesized MIL-100 with additional bands owing to coordination between the MOF and the functionalizing agent (ethylenediammine). The presence of these new bands was established by comparing them with the spectrum of an ethylenediammine functionalized MOF reported [27]. The synthesized ED-MIL-100 showed bands at 1560, 1030, and 958 $cm^{-1}$ which correlated well with the bands in ethylenediammine functionalized MOF previously reported [27]. The absorption bands observed at 1598, 1040 and 986 $cm^{-1}$ were assigned to the $\upsilon(N–H)$, $\upsilon(C-N)$, and $\upsilon(N-H_2)$ stretching vibrations respectively [27]. UV–vis spectrum (Table 3) of MIL-100 gave peaks at (27,855, 27,624, 22,272, 21,552 $cm^{-1}$) 359, 362, 449, 464 nm, the band is assigned to @→@*, n→@*, MLCT respectively [33]. The functionalized MIL-100 s i.e. TH-MIL-100 shows a shift in the bands to (27,785 $cm^{-1}$ and 22,321 $cm^{-1}$) 360 nm and 448 nm; while ED-MIL-100 shows a shift in the bands to (28,735 $cm^{-1}$ and 20,121 $cm^{-1}$) 348 nm and 497 nm depicting @→@* and MLCT respectively. The assignments are in accordance to the assignments given by Tella and Obaleye [33] in the proposed octahedral geometry of a complex. Table 2 and Fig. 2a–c presents the FT-IR absorption bands of the prepared MOFs.

### 3.3 SEM analysis

The surface morphologies and chemical compositions of the virgin and the functionalized MIL-100 samples were observed by scanning electron microscopy (SEM) and presented in Fig. 3a–c. The image of the MIL-100 before functionalization showed a smooth crystalline surface. However, upon functionalization, morphological transformation occurred and the surfaces became rough
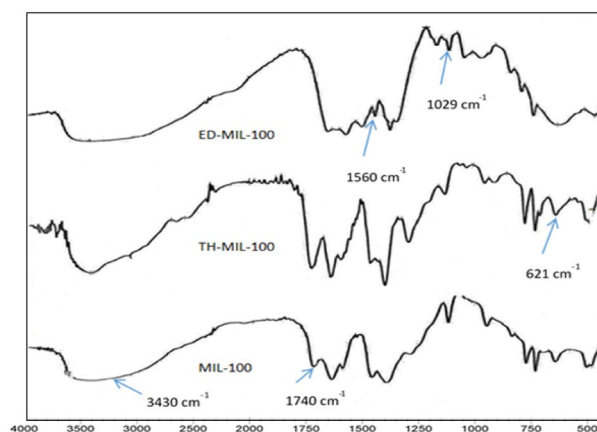


**Fig. 2** FTIR absorption bands of the adsorbents: **a** TH-MIL-100; **b** ED-MIL-100; and **c** MIL-100

suggesting that there was partial distortion of the framework during the functionalization process of the MOF [34].

### 3.4 Powder X-ray diffraction analysis results

The PXRD patterns of the MIL-100, TH-MIL-100, and ED-MIL-100 is presented in Fig. 4. The pattern of MIL-100 shows characteristic peaks at 2Θ value of 26.58°, 27.48°, and 27.98° which is comparable with values reported [17, 28]. Peak observed at 20.94° and 24.1 in the MIL-100 material was seen at 20.24°and at 24.86° in the TH-MIL-100. The PXRD pattern of the prepared materials are presented in Fig. 4.

### 3.5 BET analysis results

Measurements of the porosity and surface area of the MIL-100(Fe), TH-MIL-100, and ED-MIL-100 materials was carried out by $N_2$ adsorption experiments (Fig. 5). The BET specific surface area values were observed to be 602.516 $m^2 g^{-1}$ for MIL-100(Fe), 464.948 $m^2 g^{-1}$ for the TH-MIL-100, and 530.442 $m^2 g^{-1}$ for the ED-MIL-100. There is decrease in surface area values for the functionalized TH-MIL-100 and ED-MIL-100 materials as compared to the unfunctionalized MIL-100(Fe), this is attributed to attachment to the pore surfaces and partial blockage of the pores by thio- and
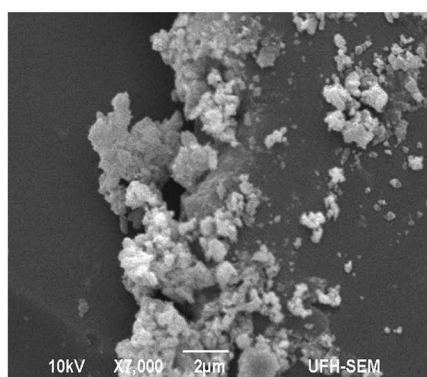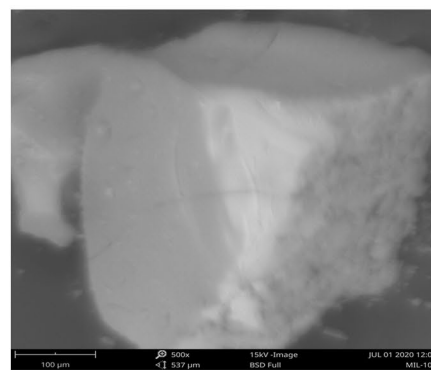
**Table 2** FTIR absorption bands of the adsorbents MIL-100, TH-MIL-100, and ED-MIL-100

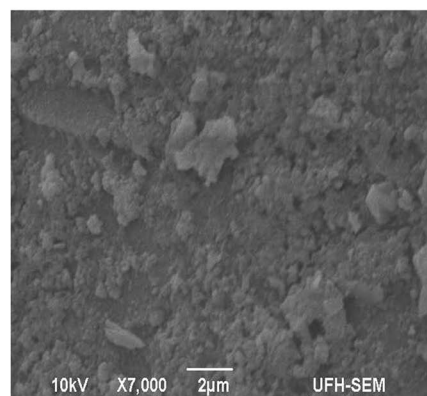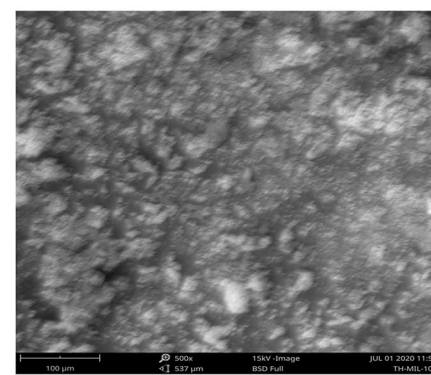| Adsorbents | Wavenumber ($cm^{-1}$) | | | | | | | | |
|---|---|---|---|---|---|---|---|---|---|
| | $\upsilon(OH)$ | $\upsilon(C=O)$ | $\upsilon(C–O)$ | $\upsilon(C=C)$ | $\upsilon(C–H)$ | $\upsilon(S–H)$ | $\upsilon(C–S)$ | $\upsilon(N–H)$ | $\upsilon(C–N)$ | $\upsilon(NH_2)$ |
| MIL-100 | 3430 | 1720 | 1382 | 1450 | 2970 | – | – | – | – | |
| TH-MIL-100 | 3425 | 1714 | 1382 | 1490 | 3000 | 2659 | 621 | – | – | |
| ED-MIL-100 | 3414 | | 1361 | 1490 | | – | – | 1560 | 1029 | |

**Fig. 3** SEM images of **a** MIL-100, **b** TH-MIL-100, **c** ED-MIL-100 at different magnification
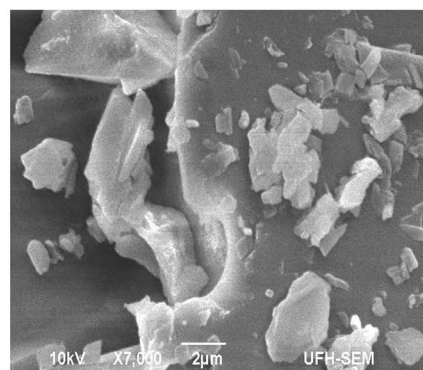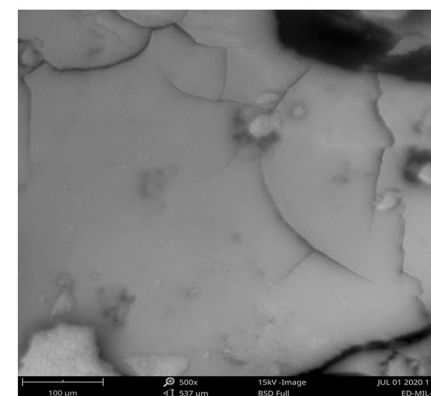


(a)      MIL-100

(b)      TH-MIL-100

(c)      ED-MIL-100

amine- groups on the materials leaving limited accessible pore volume for nitrogen molecules [32, 35, 36].

## 3.6 Results of adsorption studies

### 3.6.1 Effect of concentration

The result of the effect of concentration of the eosin B dye on the adsorption process using different adsorbents is shown in Fig. 6. The amount of the eosin B dye adsorbed on the adsorbents was observed to increase as the concentration of the dye increased reaching a maximum at 25 mg/L for MIL-100 and TH-MIL-100, and 20 mg/L for ED-MIL-100. The adsorption sites on the adsorbents were observed to become saturated as the concentration of eosin B dye increased, resulting in subsequent desorption of the dye as the process continued. Increased competition between the molecule of the eosin B dye for adsorption sites on the adsorbent resulted in an initial increase in the adsorption process followed by a subsequent slowing down of the
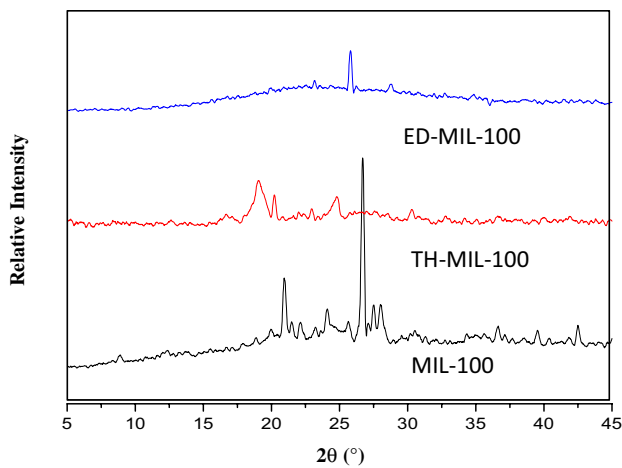
**Fig. 4** Comparison of powder X-ray diffraction (PXRD) patterns of MIL-100, TH-MIL-100, and ED-MIL-100

process [16]. This phenomenon is attributed to the fact that at a low concentration of the dye, solute to adsorbent vacant sites ratio is high, which results in an increase in the removal of the dye [16]. The result also showed that the adsorption capacities of the three adsorbents increased in the sequence of TH-MIL-100 > MIL-100 > ED-MIL-100.

### 3.6.2 Effect of time

The effect of time on the adsorption of eosin B dye onto the adsorbents shown in Fig. 7 indicates that the adsorption efficiency increased gradually with increase in contact time and reached a maximum value after 60 min for MIL-100, TH-MIL-100, and ED-MIL-100 and remained constant thereafter. The experiment was carried out at pH 8.0 using 25 mg/L dye concentration for MIL-100 and TH-MIL-100, and 20 mg/L dye concentration for ED-MIL-100; 0.02 g adsorbent dosage for 30–180 min duration in order to determine the equilibrium time for the adsorption process. The increase in adsorption at the commencement of the process is attributed to the availability of vacant adsorption sites on the adsorbents, which became occupied with time [35].

### 3.6.3 Effect of pH

Figure 8 shows the effect of pH on the adsorption of eosin B onto the adsorbents. The effect was studied using the equilibrium concentrations of dye for each of the adsorbents (i.e. 25 mg/L for MIL-100 and TH-MIL-100 and 20 mg/L for ED-MIL-100) for a period of 60 min for each experiment, while the pH was varied from 2.0 to 13.0 using 0.1 M HCl or 0.1 M NaOH. The results showed that ED-MIL-100 adsorbed more at lower pH value between
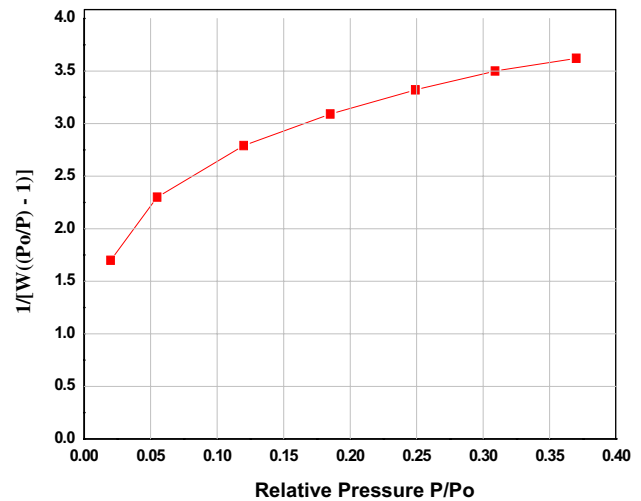


**(a)** MIL-100(Fe)
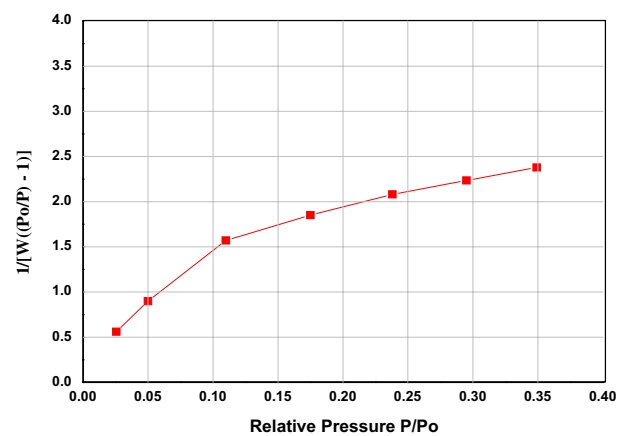


**(b)** TH-MIL-100
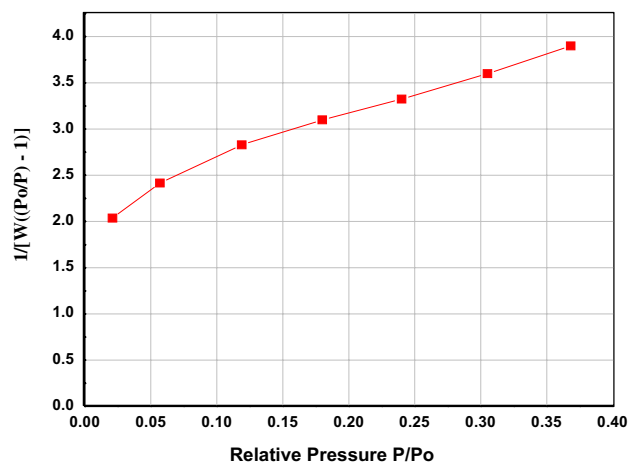


**(c)** ED-MIL-100

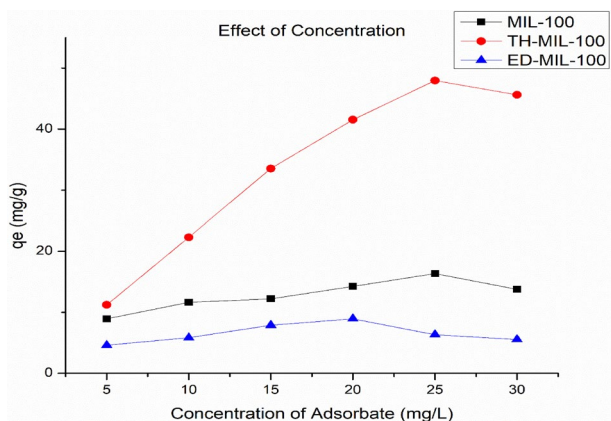**Fig. 5** BET analysis results of **a** MIL-100; **b** TH-MIL-100; and **c** ED-MIL-100

**Fig. 6** Effect of concentration on the quantity of eosin B adsorbed on the adsorbents
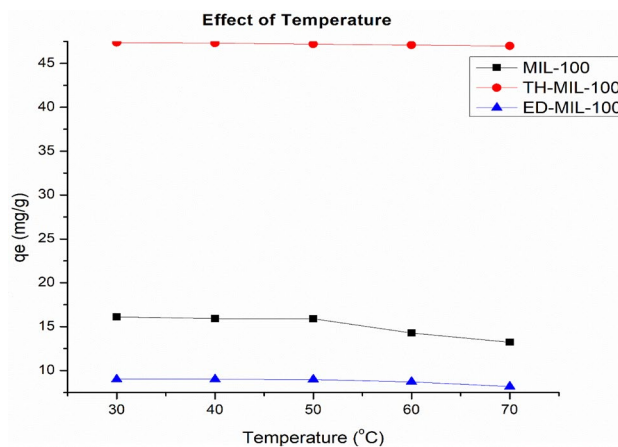


**Fig. 9** Effect of temperature on the quantity of eosin B adsorbed on the adsorbents
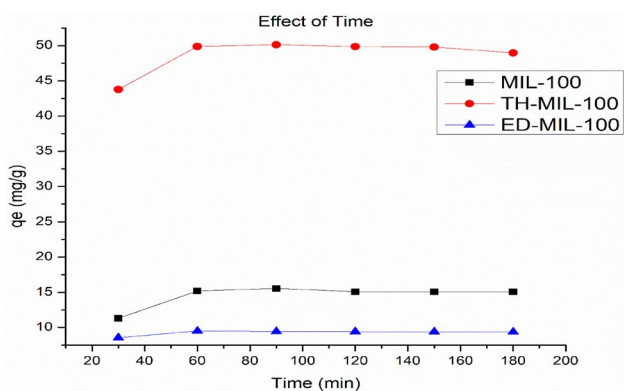


**Fig. 7** Effect of time on the quantity of eosin B adsorbed on the adsorbents
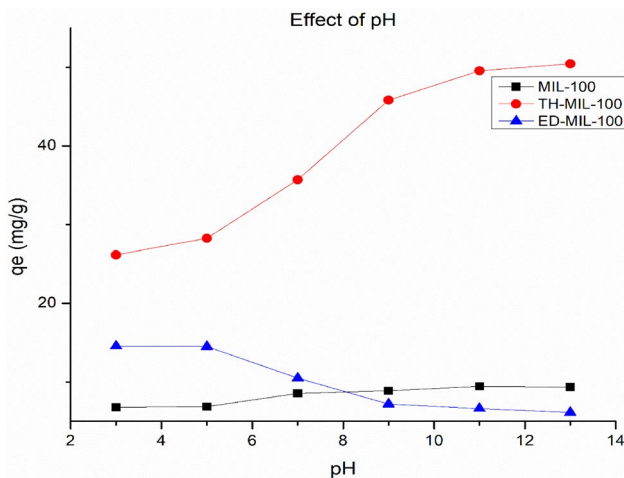


**Fig. 8** Effect of pH on the quantity of eosin B adsorbed on the adsorbents

2.0 and 5.0. This is suggested to be brought about by acid–base interaction of the dye molecules with the surface of the ED-MIL-100 adsorbent [34]. In addition, at high pH value (8.0–13.0), the eosin B dye becomes anionic in nature due to the presence of hydroxyl ions in its solution leading to an increase in the adsorption of the dye onto the surface of the TH-MIL-100 adsorbent [36].

### 3.6.4 Effect of temperature

The effect of temperature increase on the adsorption process of eosin B dye on the adsorbents was studied using the equilibrium solution concentrations of dye for each of the adsorbents (i.e. 25 mg/L for MIL-100 and TH-MIL-100, and 20 mg/L for ED-MIL-100), and 0.02 g of the adsorbent at a pH value of 2.0 for MIL-100 and ED-MIL-100, and 8.0 for the TH-MIL-100, by varying the temperature between 30 and 70 °C, for a period of 60 min for each experiment. The result of the study shown in Fig. 9 indicated that increase in temperature had very minimal effect on the adsorption process.

### 3.6.5 Effect of adsorbent dosage

The effect of adsorbent dosage on the adsorption of eosin B dye onto the adsorbents was studied using the equilibrium concentration of dye solution of 25 mg/L for MIL-100 and TH-MIL-100, and 20 mg/L for ED-MIL-100, while the amount of adsorbent used was varied from 0.01 to 0.05 g at a pH of 2.0 for MIL-100 and ED-MIL-100, and 8.0 for the TH-MIL-100 for a period of 60 min for each experiment (Fig. 10). The removal process was observed to increase as the adsorbent quantities increased due to an increase in adsorption sites amount of the adsorbents was increased which was accompanied by an increase in
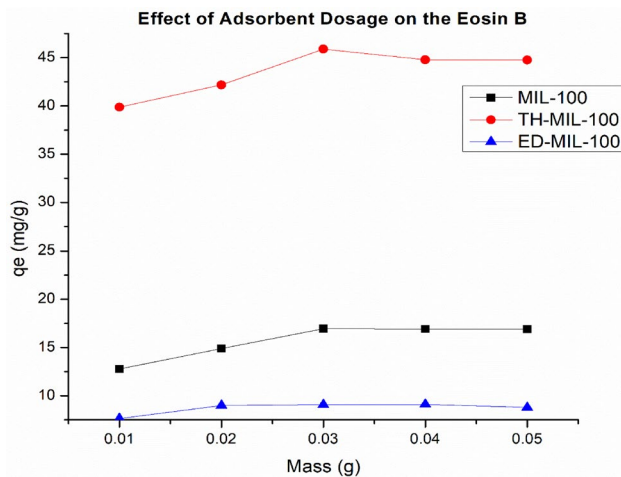
Fig. 10 Effect of adsorbent dosage on the quantity of eosin B adsorbed on the adsorbents



Fig. 11 Langmuir isotherm plot

Table 3 Wavelengths of absorbance for the adsorbents before and after adsorption

| S/N | MIL-100 adsorbents | Wavelength (nm) | |
| --- | --- | --- | --- |
| | | Before adsorption | After adsorption |
| 1 | MIL-100 | 359, 362, 464 | 393, 410, 553 |
| 2 | TH-MIL-100 | 350, 360, 488 | 354, 415, 554 |
| 3 | ED-MIL-100 | 348, 497 | 350, 544 |

adsorbents and consequently, available adsorption sites [37]. The adsorption of the eosin B dye on the MIL-100 and TH-MIL-100 reached a maximum with an adsorbent dose of 0.03 g for the process involving MIL-100 and TH-MIL-100, and 0.02 g adsorbent for the process involving ED-MIL-100.



Fig. 12 Freundlich isotherm plot

### 3.6.6 Comparison of UV–Vis spectra measurements before and after adsorption

The UV–Vis spectra of the adsorbents were obtained before and after the adsorption process, compared and the result presented in Table 3.

The results showed shifts in absorption band wavelengths of the three adsorbents after adsorption from 359 nm cm$^{-1}$, 362 nm and 464 nm to 393 nm, 410 nm and 553 nm respectively for MIL-100; 350 nm, 360 nm, and 488 nm to 354 nm, 415 nm and 554 nm respectively for TH-MIL-100; and 348 nm and 496 nm to 350 nm and 544 nm respectively for ED-MIL-100. The absorption band wavelengths shifted to higher value towards the visible region of the spectra, this is probably due to adsorption of the dye by the MOFs [38].
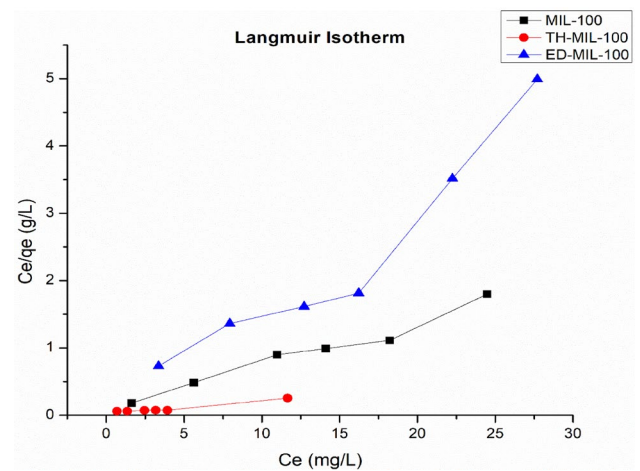
### 3.6.7 Equilibrium adsorption isotherm studies
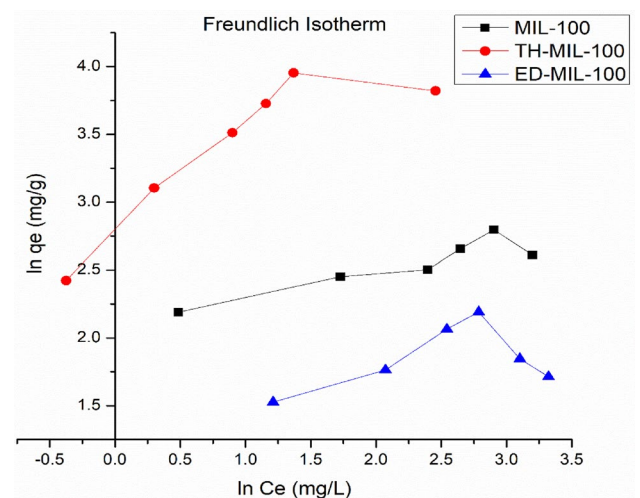
Information about adsorption mechanism can be obtained from the equilibrium adsorption isotherms using isotherms models such as Langmuir, Freundlich, Tempkin, and Dubinin–Radushkevich [D–R]. Figures 11, 12, 13, 14 shows the plot of the various isotherms for the adsorption process and the parameters of the isotherm equations summarized in Table 4.

The linear form of the Langmuir isotherm model gave the values of $K_a$ [the Langmuir adsorption constant (L/mg)] and $Q_m$ [theoretical maximum adsorption capacity (mg/g)] obtained from the intercept and slope of the plot of $C_e/Q_e$ versus $C_e$, respectively. Adsorption onto an adsorbent is assumed to be a monolayer adsorption with no interaction between the adsorbate molecules [35, 39]. Correlation
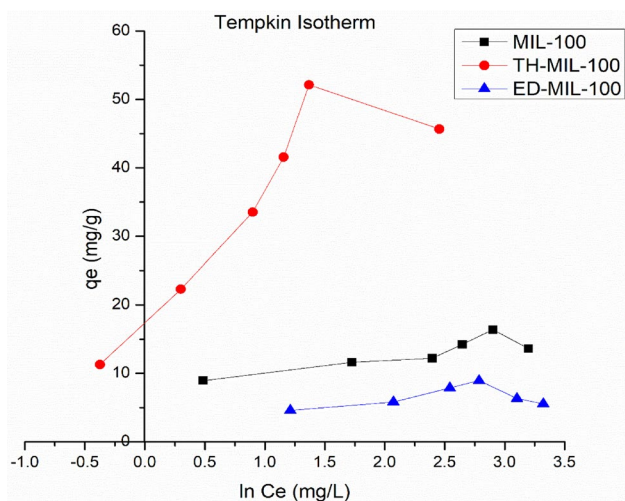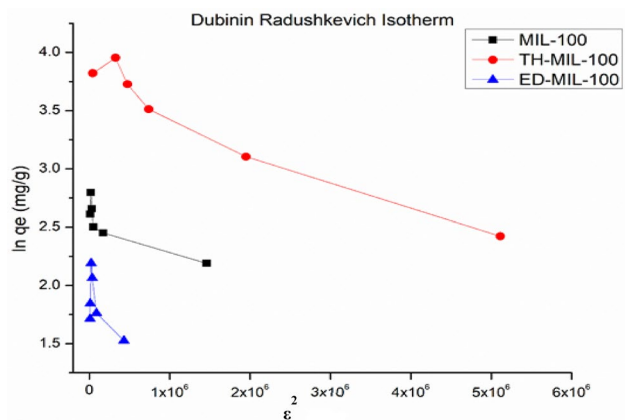
**Fig. 13** Tempkin isotherm plot



**Fig. 14** Dubinin Radushkevich plot

coefficient of between 0.9150 and 0.9676 obtained for the three MIL-100 adsorbents strongly supports the Langmuir model being most suitable for the adsorption process. The Langmuir monolayer capacity $Q_e$ of eosin B dye per gram of TH-MIL-100 adsorbent was obtained as 53.28 mg suggests that it the adsorbent shows highest relevant adsorption properties compared to MIL-100 and ED-MIL-100 which have 15.20 mg and 7.23 mg values respectively for $Q_e$. The linear form of the Langmuir model and the equation used in calculating the separation factor ($R_L$) are given in Eqs. 2 and 3 below:

$$\frac{C_e}{Q_e} = \frac{1}{K_a Q_m} + \frac{C_e}{Q_m} \tag{2}$$

$$R_L = 1/\left(1 + K_a C_o\right) \tag{3}$$

where $K_a$ (L/mg) is the Langmuir constant and $C_o$ (mg/L) is the initial concentration. The adsorption process can be determined as favorable when the $R_L$ value lies between 0 and 1 [36]. It was found that for the three MIL-100 adsorbents the $R_L$ values are lower than 1, suggesting the favorable adsorption and the fitness of Langmuir model to the experimental data.

The Freundlich isotherm model parameters such as $K_f$ [(mg g$^{-1}$)/(mg L$^{-1}$)] and $1/n$ were obtained from the intercept and slope of the linear plot of ln $q_e$ versus ln $C_e$, respectively. $K_f$ = Freundlich constant which indicates the extent of adsorption; $1/n$ = heterogeneity factor (adsorption effectiveness).

$$ln q_e = ln K_f + \frac{1}{n} ln C_e \tag{4}$$

**Table 4** Comparison of the coefficients isotherm parameters for eosin B adsorption onto the MIL-100 s adsorbents

| Isotherms | Equations | Constants | Adsorbents | | |
|---|---|---|---|---|---|
| | | | MIL-100 | TH-MIL-100 | ED-MIL-100 |
| LANGMUIR | $C_e/q_e = 1/K_a Q_e + C_e/Q_e$ | Qe (mg/g) | 15.20 | 53.48 | 7.23 |
| | | $K_a$ (L mg$^{-1}$) | 0.74 | 0.67 | 0.80 |
| | | $R_L$ | 0.05 | 0.06 | 0.06 |
| | | $R^2$ | 0.9676 | 0.9537 | 0.9150 |
| FREUNDLICH | $\ln q_e = \ln K_f + (1/n) \ln C_e$ | $K_f$ | 8.23 | 18.60 | 4.36 |
| | | n | 5.22 | 1.93 | 6.64 |
| | | 1/n | 0.19 | 0.52 | 0.15 |
| | | $R^2$ | 0.8334 | 0.7595 | 0.2293 |
| | | $B_1$ (mg/g) | 2.26 | 13.81 | 1.10 |
| TEMPKIN | $q_e = B_I \ln K_T + B_I \ln C_e$ | $K_T$ | 31.81 | 4.99 | 134.08 |
| | | $R^2$ | 0.7714 | 0.7572 | 0.1784 |
| DUBININ-RADUSHKEVIC | $\ln q_e = \ln Q_s - B\varepsilon^2$ | Qs | 13.78 | 46.64 | 7.02 |
| | | E (KJ/mol) | 408.25 | 235.70 | 500 |
| | | B | $-3.0 \times 10^{-6}$ | $-9.0 \times 10^{-6}$ | $-1 \times 10^{-6}$ |
| | | $R^2$ | 0.7237 | 0.9451 | 0.4459 |

The 1/$n$ value of 0.15–0.52 obtained indicates the favorable adsorption and high tendency of eosin B dye for adsorption onto the unfunctionalized and functionalized MIL-100(Fe) adsorbents, while lower $R^2$ values (0.2293–0.8334) for the adsorbents indicates that the Freundlich model less fits the experimental data [35, 37].

The heat of the adsorption and the adsorbent–adsorbate interaction was evaluated using Tempkin isotherm model. In this model, $B_l$ is the Tempkin constant related to heat of the adsorption (J/mol), $T$ is the absolute temperature (K), $R$ is the universal gas constant (8.314 J/mol/K) and $K_T$ is the equilibrium binding constant (L/mg). The values of the Tempkin constants (1.10–2.26) and the correlation coefficient (0.1784–0.7714) are lower than the Freundlich and Langmuir values, indicating that the Tempkin isotherm is a lesser fit for the experimental data than both Langmuir and Freundlich isotherms.

$$q_e = B_l ln K_T + B_l ln C_e \qquad (5)$$

The Dubinin Radushkevich model was applied to estimate the porosity apparent free energy and the characteristic of adsorption. In this model, K (mol$^2$/(kJ$^2$)) is a constant related to the adsorption energy, $Q_s$ (mg/g) is the theoretical saturation capacity, and $e$ is the Polanyi potential. The slope of the plot of ln $q_e$ versus $\varepsilon^2$ gives $K$ and the intercept gives the $Q_s$ value. The D–R equation was seen to represent a poor fit for the experimental data for MIL-100 and ED-MIL-100 but suitable for TH-MIL-100.

$$ln q_e = ln Q_s - B_{\varepsilon^2} \qquad (6)$$

The correlation coefficient of the Langmuir isotherm was observed to be higher than that of the other isotherms, which suggests that the adsorption process of eosin B dye onto the three adsorbents can better be described with the Langmuir model and the adsorption is a monolayer adsorption in addition to Dubinin Radushkevich model which fits in for TH-MIL-100 [40–42].

### 3.6.8 Adsorption kinetic

The pseudo-first- and second-order kinetics, Elovich and intraparticle diffusion models were used to study the rate and mechanism of adsorption process, and the results are presented in Table 5 with the equations for the models. The pseudo-first-order model (Lagergren model) was obtained by a plot of the values of log ($q_e$–$q_t$) versus time, and values of $k_1$ and $q_e$ were determined from the slope and intercept of the graph respectively (Fig. 15). The difference between the intercept and the experimental $q_e$ value indicates that this model does not explain the experimental data and rate of adsorption does not follow this equation [42, 43]. The validity of the model was further checked by the correlation coefficient ($R^2$). The low $R^2$ values again
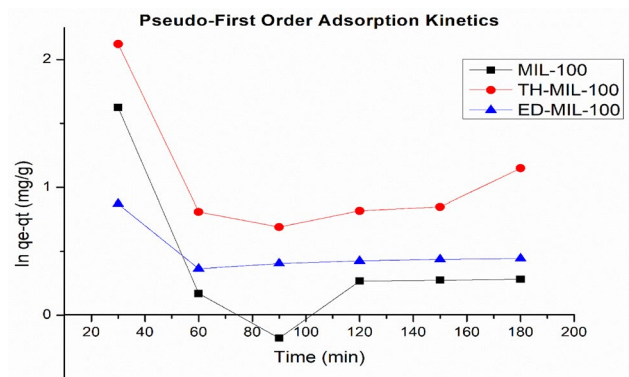


**Fig. 15** Pseudo- first order adsorption kinetics

**Table 5** Kinetic parameters of eosin B adsorption onto MIL-100 s

| Models | Equations | Parameters | Adsorbents | | |
|---|---|---|---|---|---|
| | | | MIL-100 | TH-MIL-100 | ED-MIL-100 |
| First-order kinetic model | $ln(q_e - q_t) = ln(q_e) - K_1 t$ | $K_1$ | 0.0054 | 0.045 | 0.0018 |
| | | $q_e$ (cal) | 2.98 | 4.40 | 1.98 |
| | | $R^2$ | 0.2610 | 0.212 | 0.2881 |
| Second-order kinetic model | $t/q_t = 1/k_2 q_e^2 + (1/q_e)t$ | $q_e$ (cal) | 15.77 | 49.50 | 9.50 |
| | | $R^2$ | 0.9953 | 0.9986 | 0.9995 |
| | | $K_2$ | 0.011 | 0.017 | 0.076 |
| Intraparticle diffusion | $q_t = K_{idiff} t^{1/2} + C$ | C | 10.84 | 43.406 | 8.5045 |
| | | $K_{diff}$ | 0.3712 | 0.5389 | 0.079 |
| | | $R^2$ | 0.469 | 0.4161 | 0.4215 |
| Elovich | $q_t = 1/\beta \ln(\alpha\beta) + 1/\beta \ln(t)$ | $B$ | 0.1604 | 0.3659 | 2.5107 |
| | | $R^2$ | 0.5913 | 0.5428 | 0.5399 |
| Experimental Adsorption Capacity ($q_e$) | | | 16.35 | 47.96 | 8.95 |

showed that the pseudo-first-order model does not fit well with the experimental data.

The plot of $t/q_t$ versus $t$ for the pseudo-second-order kinetic model gave a straight line with a high correlation coefficient ($R^2$) (Fig. 16). The $k_2$ and equilibrium adsorption capacity ($q_e$) were calculated from the intercept and slope of this line, respectively. The high values of $R^2$ (0.99) and closeness of experimental and theoretical adsorption capacity ($q_e$) value show the applicability of the pseudo-second-order model to explain and interpret the experimental data [42, 43]. The intra-particle diffusion model is shown in Fig. 17.

The intraparticle diffusion model based on diffusive mass transfer that adsorption rate can be expressed in terms of the square root of time ($t$) [44–48] was also applied. The values of $K_{diff}$ [the intraparticle diffusion rate constant (mg/g/min$^{1/2}$)] and $C$ (thickness of the boundary layer) were calculated from the slope and intercept of the plot of $q_t$ versus $t^{1/2}$ respectively (Fig. 17) and the results are presented in Table 5.

The Elovich equation is another rate equation based on the adsorption capacity in linear form, which has been successfully applied for the adsorption of solutes from a liquid solution [44, 45]. The plot of $q_t$ versus ln ($t$) gives a linear relationship (Fig. 18) with a slope of (1/$b$) and an intercept of (1/$b$)ln($ab$). The Elovich constants obtained from the slope and the intercept of the straight line are reported in Table 5. The correlation coefficients ($R^2$) were observed to be low showing that this model is unsuitable for complete evaluation of the adsorption process [44].

From the results in Table 5, it is obvious that the adsorption of the dye followed the pseudo-second-order kinetics. The theoretical values obtained were close to experimental values with correlation coefficients > 0.99, which fitted better than the other kinetic models for the entire adsorption process. Therefore, it can be concluded that
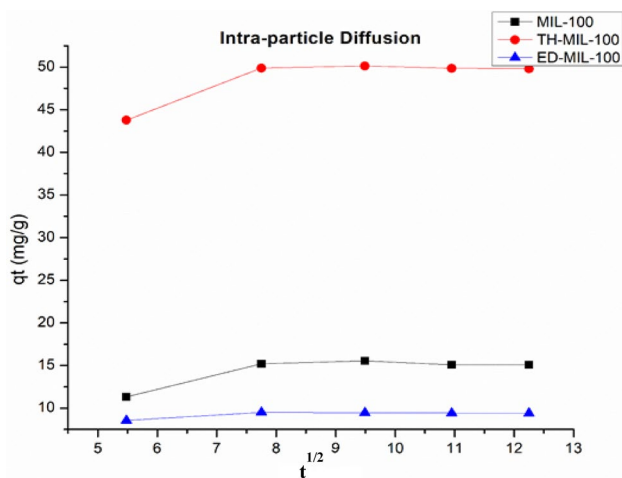


**Fig. 17** Intra particle diffusion kinetics

pseudo-second-order equation is better in describing the adsorption kinetics of eosin B on MIL-100 adsorbents and therefore the rate of reaction appeared to be controlled by the chemical interaction [47–52].

### 3.6.9 Adsorption Mechanism

The surface area of the three adsorbents are in order of MIL-100 > > ED-MIL-100 > TH-MIL-100 but the adsorption capacities were in order of TH-MIL-100 > MIL-100 > ED-MIL-100. Contrary to the rule, the materials with large surface are expected to have excellent adsorption, but it is interesting to note that TH-MIL-100 with lowest surface area has highest adsorption, this indicates that porosity/surface area is not the only factor determines adsorption capacity. It can be observed that functionalization of MIL-100 with thioglycolic acid and ethylenediamine generates acidic $SO_3H$ and basic $NH_2$. The only possible
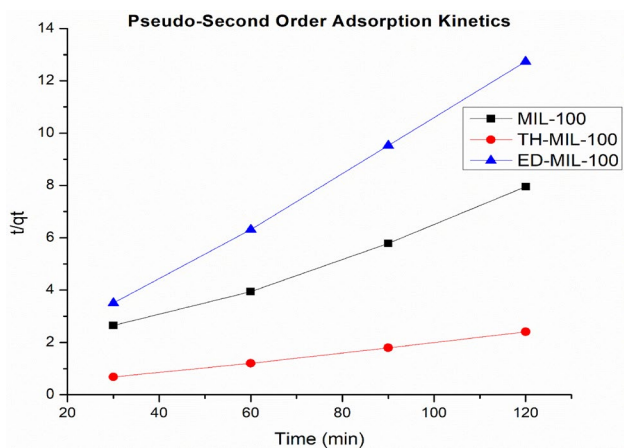


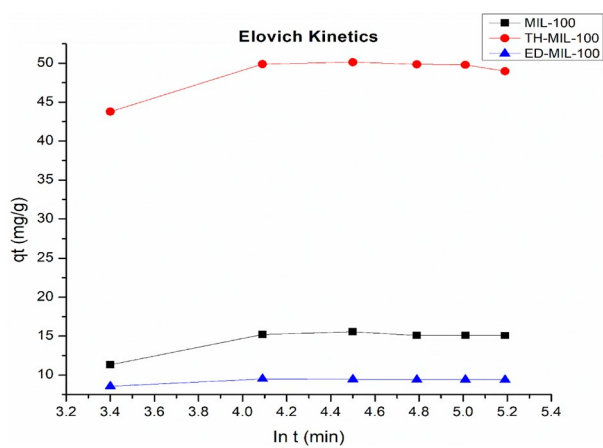**Fig. 16** Pseudo-second order adsorption kinetics



**Fig. 18** Elovich kinetics

mechanism that can explain the highest adsorption capacity of TH-MIL-100 for Eosin-B is therefore electrostatic interaction between the positive charged surface of TH-MIL-100 via incorporation of thioglycolic acid and anionic dye(negatively charged). The acidic TH-MIL-100 may result to acid–base interaction during the adsorption of the eosin-B dye because of the acidity of the adsorbent and the $COO^-$ of the eosin-B.

However for ED-MIL-100 with $NH_2$ group has the lowest adsorption, because of electrostatic repulsion between the basic group (negatively charged) of the ED-MIL-100 and the anionic dye (eosin –B). Similar findings were also reported previous [53–56]. Thus the adsorption capacity follows the order TH-MIL-100 > MIL-100 > ED-MIL-100.

**3.6.9.1 Comparison of adsorption capacity** The adsorption of capacity of the materials prepared were compared with that obtained by other researchers for the removal of eosin B dye from the environment and presented in Table 6. It was observed that the prepared materials compared favourably well with other materials prepared in similar researches.

**3.6.9.2 Reusability experiments** The reusability of the MIL-100(Fe) and the functionalized MIL-100(Fe) materials for the removal of eosin B dye from aqueous medium was investigated for each compound. The optimum conditions of 25 mg/L for MIL-100 and TH-MIL-100; and 20 mg/L for ED-MIL-100, equilibrium time of 60 min, and optimum pH of 13 for TH-MIL-100 and MIL-100; and at pH of 2 for ED-MIL-100 materials, and adsorbent doses of 0.03 g for MIL-100 and TH-MIL-100; and 0.02 g for ED-MIL-100 were employed for the reusability experiments. The percentage removal was calculated using the calibration curve and absorbance value obtained. The results indicated that the materials can be reused as adsorbents for the removal of eosin B dye from aqueous medium for more than three runs with decreasing value of removal efficiency for each run (Fig. 19).

**Table 6** Comparison of adsorption capacities obtained for the removal of eosin B dye

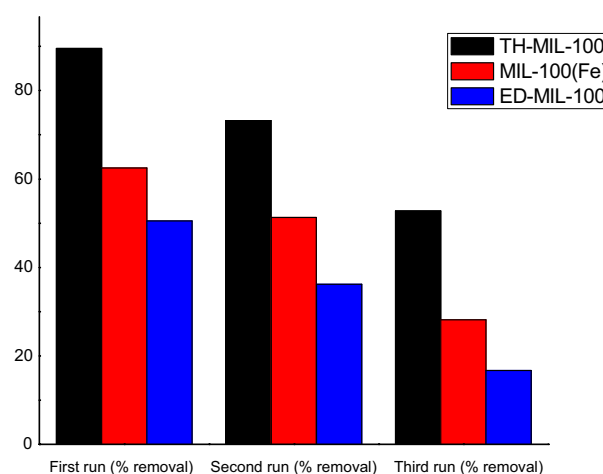| Researcher | $Q_e$ (mg/g) |
| --- | --- |
| This work | 53.28 |
| Mehmood et al. [54] | 16.28 |
| Kant [55] | 48.8 |
| Kanwal et al. [56] | 7.96 |



**Fig. 19** Reusability experiments

## 4 Conclusion

The low-cost metal–organic frameworks (MIL-100(Fe) were prepared using simple synthesis route. The synthesized MOFs were used as adsorbents for the removal of eosin B dye from aqueous solution. The results showed that the synthesized MOFs have high adsorption capacity for eosin B dye. The adsorption process was fast and reached equilibrium within 90 min. The TH-MIL-100 was found to be the most effective in the removal of eosin B, due to the presence of the thio- group on the TH-MIL-100 material as observed in the results of the BET analysis carried out. The acid–base interaction between the adsorbent and the adsorbate due to the presence of thioglycolic acid molecules which made the MOF acidic is also suggested as improving the removal efficiency. Langmuir isotherm gave a better fit to adsorption isotherms. The kinetic study of eosin B onto MIL-100 s adsorbents indicated that the adsorption kinetics followed the pseudo-second-order rate. Optimum conditions obtained for maximum adsorption of eosin B dye on the adsorbents were observed to be at dye concentrations of 25 mg/L for MIL-100 and TH-MIL-100, and 20 mg/L for ED-MIL-100. The equilibrium time for maximum adsorption was observed to be 60 min, while optimum pH was observed to be 13 for TH-MIL-100 and MIL-100, and at pH of 2 for ED-MIL-100. Increase in temperature was observed to have no appreciable effect on the adsorption process, while the maximum adsorption capacity was observed for adsorbent doses of 0.03 g for MIL-100 and TH-MIL-100, and at 0.02 g for ED-MIL-100. The results of this study suggest that low cost MOFs obtained using simple approach like ours could be utilized as effective adsorbents for the adsorption of dyes from wastewater.

## Compliance with ethical standards

## References

1. Eddaoudi M, Li H, Yaghi OM (2000) Highly porous and stable metal-organic frameworks: structure design and sorption properties. J Am Chem Soc 122:1391–1397

2. Chae HK, Siberio-Perez DY, Kim J, Go YB, Eddaoudi M, Matzger AJ, O'Keeffe M, Yaghi OM (2004) A route to high surface area, porosity and inclusion of large molecule in crystal. Nature 427:523–527

3. Murray LJ, Dinca M, Long JR (2009) Hydrogen storage in metal organic frameworks. Chem Soc Rev 38:1294–1314

4. Morris RE, Wheatley PS (2008) Gas storage in nanoporous materials. Angew Chem Int Ed 47:4966–4981

5. Li JR, Kuppler RJ, Zhou HC (2009) Selective gas adsorption and separation in metal organic frameworks. Chem Soc Rev 38:1477–1504

6. Meilikhov M, Yusenko K, Esken D, Turner S, Van Tendeloo G, Fischer RA (2010) Metals@MOFs—loading MOFs with metal nanoparticles for hybrid functions. Eur J Inorg Chem 24:3701–3714

7. Müller M, Hermes S, Kähler K, Van-den Berg MWE, Muhler M, Fischer RA (2008) Loading of MOF-5 with Cu and ZnO nanoparticles by Ggs-phase infiltration with organometallic precursors: properties of Cu/ZnO@MOF-5 as catalyst for methanol synthesis. Chem Mater 20:4576–4587

8. Lee J, Farha OK, Roberts J, Scheidt KA, Nguyen ST, Hupp JT (2009) Metal organic framework materials as catalysts. Chem Soc Rev 38:1450–1459

9. Ma L, Abney C, Lin W (2009) Enantioselective catalysis with homochiral metal organic frameworks. Chem Soc Rev 38:1248–1256

10. McKinlay AC, Morris RE, Horcajada P, Férey G, Gref R, Couvreur P, Serre C (2010) Metal-organic frameworks for biological and medical applications. Angew Chem Int Ed 49:6260–6266

11. Horcajada P, Serre C, Maurin D, Ramsahye NA, Balas F, Vallet-Regi M, Sebban M, Taulelle F, Ferey G (2008) Flexible porous metal-organic frameworks for a controlled drug delivery. J Am Chem Soc 130:6774–6780

12. Horcajada P, Serre C, Vallet-Regi M, Sebban M, Taulelle F, Ferey G (2008) Metal-organic frameworks as efficient materials for drug delivery. Angew Chem Int Ed 45:5974–5978

13. Huxford RC, Della JR, Lin W (2010) Metal-organic frameworks as potential drug carriers. Curr Opin Chem Biol 14:262–268

14. Tanabe KK, Cohen SM (2011) Postsynthetic modification of metal-organic frameworks- a progress report. Chem Soc Rev 40(2):498–519

15. Keenan LL (2014) Post-synthetic modification of metal-organic frameworks. Ph.D. Thesis, University of Bath.

16. Afkhami A, Tehrani MS, Bagheri H (2010) Modified maghemite nanoparticles as an efficient adsorbent for removing some cationic dyesfrom aqueous solution. Desal 263:240–248

17. Horcajada P, Surble S, Serre C, Hong DY, Seo YK, Chang JS, Greneche JM, Margiolaki I, Férey G (2007) Synthesis and catalytic properties of MIL-100(Fe), an iron(III) carboxylate with large pores. Chem Commun 75:2820–2822

18. Hamedi A, Zarandi MB, Nateghi MR (2019) Highly efficient removal of dye pollutants by MIL-101(Fe) metal-organic framework loaded magnetic particles mediated by Poly L-Dopa. J Environ Chem Eng 7:102882

19. Hamedi A, Trotta F, Zarandi MB, Zanetti M, Caldera F, Anceschi A, Nateghi MR (2019) In Situ Synthesis of MIL-100(Fe) at the surface of $Fe_3O_4$@AC as highly efficient dye adsorbing nanocomposite. Int J Mol Sci. https://doi.org/10.3390/ijms20225612

20. Kong G-Q, Ou S, Zou C, Wu C-D (2012) Assembly and post-modification of a metal–organic nanotube for highly efficient catalysis. J Am Chem Soc 134:19851–19857

21. Grunker R, Bon V, Heerwig A, Klein N, Muller P, Stoeck U, Baburin IA, Mueller U, Senkovska I, Kaskel S (2012) Dye encapsulation inside a new Mesoporous metal–organic framework for multifunctional solvatochromic-response function. Chem-A Eur J 23:12559–12564

22. Hong Y-s, Sun S-l, Sun Q, Gao E-Q, Ye M (2020) Tuning adsorption capacity through ligand pre-modification in functionalized Zn-MOF analogues. Mater Chem Phys 243:122601

23. Masoomi MY, Bagheri M, Morsali A (2016) High efficiency of mechanosynthesized Zn-based metal–organic frameworks in photodegradation of congo red under UV and visible light. RSC Adv 6:13272–13277

24. Abdollahi N, Masoomi MY, Morsali A, Junk PC, Wang J (2018) Sonochemical synthesis and structural characterization of a new Zn(II) nanoplate metal–organic framework with removal efficiency of Sudan red and Congo red. Ultrason Sonochem 45:50–56

25. Mehrorangm G, Amin A, Payman A, Abdolmohammad G, Azam V, Mohammad H (2015) Artificial neural network and bees algorithm for removal of eosin B using cobalt oxide nanoparticle-activated carbon: isotherm and kinetics study. Environ Progress Sus Energy 34:155–168

26. Manoj KRP, Rama RB, Karuppiah J, Linga RE, Subrahmanyam Ch (2013) Degradation and mineralization of methylene blue by dielectric barrier discharge non-thermal plasma reactor. Chem Eng J 217:41–47

27. Manoj KRP, Mahammadunnisa SK, Ramaraju B, Sreedhar B, Subrahmanyam Ch (2013) Low-cost adsorbents from bio-waste for the removal of dyes from aqueous solution. Environ Sci Pol Res 20:4111–4124

28. Zhang F, Shi J, Jin Y, Fu Y, Zhong Y, Zhu W (2014) Facile synthesis of MIL-100(Fe) under HF-free conditions and its application in the acetalization of aldehydes with diols. Chem Eng J 259:183–190

29. Jhung SH, Choi E, Hasan Z (2013) Adsorption of naproxen and clofibric acid over a metal-organic framework MIL-101 functionalized with acidic and basic groups. Chem Eng J 219:537–544

30. Jhung SH, Hasan Z, Jung BK (2013) Adsorptive removal of 2,4-dichlorophenoxyacetic acid (2,4-D) from water with a metal-organic framework. Chem Eng J 234:99–105

31. Jhung SH, Jeon J, Hasan Z (2012) Adsorptive removal of naproxen and clofibric acid from water using metal-organic frameworks. J Hazard Mater 209–210:151–157

32. Fei K, Qiu L, Yuan Y, Peng F, Jiang X, Xie A, Shen Y, Zhu J (2011) Thiol-functionalization of metal-organic famework by a facile coordination-based postsynthetic strategy and enhanced removal of $Hg^{2+}$ from water. J of Hazard Mater 196:36–43

33. Tella AC, Obaleye JA (2010) Metal complexes as antibacterial agents: synthesis, characterization and antibacterial activity of some 3d metal complexes of sulphadimidine Orbital. Elec J Chem Campo Grande 2(1):11–26

34. Lee HJ, We J, Kim JO, Kim D, Cha W, Lee E, Sohn J, Oh M (2015) Morphological and structural evolutions of metal-organic framework particles from amorphous spheres to crystalline hexagonal rods. Angew Chem Int Ed Engl 54(36):10564–10568

35. Tella AC, Eliagwu SE, Amali M, Kola-Mustapha AT, Olatunji SJ, Ishola F, Adimula VO, Oluwafemi OS (2020) Synthesis, characterization of amino and cyano functionalized zinc terephthalate metal-organic frameworks for loading of piroxicam drugs. Chem Pap 74:2287–2296

36. Tella AC, Owalude SO, Ojekanmi CA, Oluwafemi OS (2014) Synthesis of copper-isonicotinate metal-organic frameworks simply by mixing solid reactants and investigation of its adsorptive properties in the removal of fluorescein dye. New J Chem 38:4494–4500

37. Elaigwu SE, Rocher V, Kyriakou G, Greenway GM (2014) Removal of $Pb^{2+}$ and $Cd^{2+}$ from aqueous solution using chars from pyrolysis and microwave-assisted hydrothermal carbonization of *Prosopis africana* shell. J Indus Eng Chem 205:3467–3473

38. Litefti K, Freire MS, Stitou M, Gonzalez-Alvarez J (2019) Adsorption of an anionic dye (Congo red) from aqueous solutions by pine bark. Sci Rep 9:16530. https://doi.org/10.1038/s41598-019-53046-z

39. Ghaedi M, Ghaedi AM, Abdi F, Roosta M, Vafaei A, Asghari A (2013) Principal component analysis- adaptive neuro-fuzzy inference system modeling and genetic algorithm optimization of adsorption of methylene blue by activated carbon derived from *Pistacia khinjuk*. Ecotoxicol Environ Safety 96:110–117

40. Ravanan M, Ghaedi M, Ansari A, Taghizadeh F, Elhamifar D (2014) Comparison of the efficiency of Cu and silver nanoparticle loaded on supports for the removal of Eosin Y from aqueous solution: kinetic and isotherm study. Spectrochimica Acta Part A: Mol Biomol Spec 123:467–472

41. Mittal A, Jain R, Mittal J, Shrivastava M (2010) Adsorptive removal of hazardous dye quinoline yellow from waste water using coconut-husk as potential adsorbent. Fresenius Environ Bull 19(6):1–9

42. Dubinin MM (1960) The potential theory of adsorption of gases and vapors for adsorbents with energetically non-uniform surface. Chem Rev 60:235–266

43. Radushkevich LV (1949) Potential theory of sorption and structure of carbons. Zh Fiz Khim 23:1410–1420

44. Lagergren S (1898) Zur theorie dersogenannten adsorption geloster stoffe kungliga svenska vetenskapsakademiens. Handlingar 24:1–39

45. Ho YS (2006) Review of second-order models for adsorption systems. J Hazard Mater 136:681–689

46. Ruthven DM, Loughlin KF (1971) The effect of crystallite shape and size distribution on diffusion measurements in molecular sieve. Chem Eng Sci 26:577–584

47. Ho YS, McKay G (1999) Pseudo-second order model for sorption processes. Process Biochem 34:451–456

48. Bulut E, Ozacar M (2008) Adsorption of malachite green onto bentonite: Equilibrium and kinetic studies and process design. Micro Meso Mater 115:234–246

49. Chien SH, Clayton WR (1980) Application of Elovich equation to the kinetics of phosphate release and sorption on soils. Soil Sci Soc American J 44:265–268

50. Ghaedi M, Biyareh MN, Nasiri KS, Shamsaldini S, Sahraei R, Daneshfar A, Shahriyar S (2012) Comparison of the efficiency of palladium and silver nanoparticles loaded on activated carbon and zinc oxide nano rods loaded on activated carbon as new adsorbents for removal of Congo red from aqueous solution: kinetics and isotherm study. Mater Sci Eng C 32:725–734

51. Ozdes D, Duran C, Senturk HB (2011) Adsorptive removal of Cd(II) and Pb(II) ions from aqueous solutions by using Turkish illitic clay. J Env Man 92:3082–3090

52. Tella AC, Oladipo AC, Adimula VO, Ameen OA, Bourne SA, Ogunlaja AS (2019) Synthesis and crystal structures of a copper(II) dinuclear complex and zinc(II) coordination polymers as materials for efficient oxidative desulfurization of dibenzothiophene. New J Chem 43:14343–14354

53. Wei F, Chen D, Liang Z, Zhao S (2018) Comparison study on the Adsorption capacity of Rhodamine B, Congo Red, and Orange II on Fe-MOFs. Nanomaterials (basel) 8(4):248

54. Mehmood A, Bano S, Fahim A, Parveen R, Khurshid S (2015) Efficient removal of crystal violet and eosin B from aqueous solution using Syzygium cumini leaves: a comparative study of acidic and basic dyes on a single adsorbent. Korean J Chem Eng 32:882–895

55. Kant R (2012) Adsorption of dye eosin from an aqueous solution on two different samples of activated carbon by static batch method. J Water Res Protect 4:93–98

56. Kanwal F, Rehman R, Mustaq WM, Batool A, Naseem S (2013) Use of *opuntia dillenii* seeds for sorptive removal of acidic textile dyes from water in benign way. Asian J Chem 25(14):7710–7714